AFML-TR-71-79

AN EXPERIMENTAL METHOD FOR DETERMINING MECHANICAL PROPERTIES AT HIGH STRAIN RATES

PER MADSEN AND FRITHIOF I. NIORDSON

DEPARTMENT OF SOLID MECHANICS
THE TECHNICAL UNIVERSITY OF DENMARK, LYNGBY, DENMARK

TECHNICAL REPORT AFML-TR-71-79

MAY 1971

AIR FORCE MATERIALS LABORATORY
AIR FORCE SYSTEMS COMMAND
WRIGHT PATTERSON AIR FORCE BASE, OHIO

BLANK PAGE

NOTICE

When Government drawings, specifications, or other data are used for any purpose other than in connection with a definitely related Government procurement operation, the United States Government thereby incurs no responsibility nor any obligation whatsoever; and the fact that the government may have formulated, furnished, or in any way supplied the said drawings, specifications, or other data, is not to be regarded by implication or otherwise as in any manner licensing the holder or any other person or corporation, or conveying any rights or permission to manufacture, use, or sell any patented invention that may in any way be related thereto.

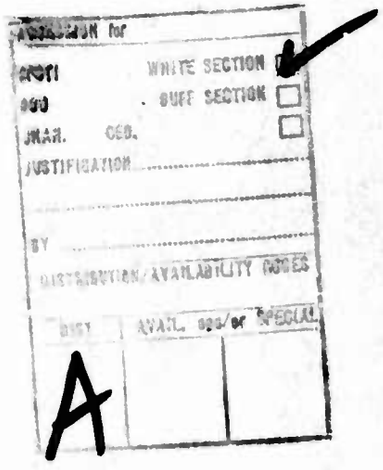

Copies of this report should not be returned unless return is required by security considerations, contractual obligations, or notice on a specific document.

400 - June 1971 - CO305 - 42-71-713

UNCLASSIFIED

Security Classification

DOCUMENT CONTROL DATA - R & D

(Security classification of title, body of abstract and indexing annotation must be entered when the overall report is classified)

1. ORIGINATING ACTIVITY (Corporate author)	2a. REPORT SECURITY CLASSIFICATION
Department of Solid Mechanics The Technical University of Denmark 2800 Lyngby	Unclassified 2b. GROUP

3. REPORT TITLE

AN EXPERIMENTAL METHOD FOR DETERMINING MECHANICAL PROPERTIES AT HIGH STRAIN RATES

4. DESCRIPTIVE NOTES (Type of report and inclusive dates)

Final Report - 1 March 1968 through 30 June 1970

5. AUTHOR(S) (First name, middle initial, last name)

Per Madsen
Frithiof I. Niordson

6. REPORT DATE	7a. TOTAL NO. OF PAGES	7b. NO. OF REFS
May 1971	47	9

8a. CONTRACT OR GRANT NO.	9a. ORIGINATOR'S REPORT NUMBER(S)
F61052-68-C-0032 b. PROJECT NO. 7351 c. TASK NO. 735106 d.	9b. OTHER REPORT NO(S) (Any other numbers that may be assigned this report) AFML-TR-71-79

10. DISTRIBUTION STATEMENT

Approved for public release; distribution unlimited

11. SUPPLEMENTARY NOTES	12. SPONSORING MILITARY ACTIVITY
	Air Force Materials Laboratory (LLD) Air Force Systems Command Wright-Patterson Air Force Base, Ohio

13. ABSTRACT

An experimental method for determining the stress-strain relation in uniform tension at very high strain rates is presented. The equipment and the measuring technique used are described in some detail together with the numerical procedures involved in evaluating the data obtained during a test. Results obtained for commercially available copper in original and in annealed conditions are presented in order to illustrate the method.

DD FORM 1 NOV 65 1473

UNCLASSIFIED

Security Classification

14 KEY WORDS	LINK A		LINK B		LINK C	
	ROLE	WT	ROLE	WT	ROLE	WT
High strain rates						
Stress-strain relation						
Experimental method						
Copper						

AN EXPERIMENTAL METHOD FOR DETERMINING MECHANICAL PROPERTIES AT HIGH STRAIN RATES

PER MADSEN AND FRITHIOF I. NIORDSON

FOREWORD

This report was prepared by the Department of Solid Mechanics, The Technical University of Denmark, Lyngby, Denmark under USAF Contract No. F61052-68-C-0032. This contract was initiated under Project No. 7351, "Metallic Materials," Task No. 7351, "Behavior of Metals." The contract was administered by the European Office, Office of Aerospace Research. The work was monitored by the Metals and Ceramics Division, Air Force Materials Laboratory, Air Force Systems Command, Wright-Patterson AFB, Ohio, with Dr. T. Nicholas (AFML/LLD), as Project Scientist.

This report covers work conducted during the period 1 March 1968 to 30 June 1970. The report was submitted by the authors 23 March 1971.

This technical report has been reviewed and is approved.

W. J. TRAPP
Chief, Strength and Dynamics Branch
Metals and Ceramics Division
Air Force Materials Laboratory

ABSTRACT

An experimental method for determining the stress-strain relation in uniform tension at very high strain rates is presented. The equipment and the measuring technique used are described in some detail together with the numerical procedures involved in evaluating the data obtained during a test. Results obtained for commercially available copper in original and in annealed condition are presented in order to illustrate the method.

CONTENTS

LIST OF ILLUSTRATIONS

BLANK PAGE

I. INTRODUCTION

It is well known that the mechanical properties of most materials are strongly dependent on the rate of strain (Ref. 1-3). This fact is of considerable interest to both the engineer and the physicist. The literature on experimental investigations of material behaviour at high strain rates is mostly concerned with the use of the so-called split-Hopkinson-bar method (Ref. 4-7). A review of earlier work in this field is not intended here, a fairly good survey being available in Ref. (8). Our main objection to the split-Hopkinson-bar method and similar techniques is that due to inertia and end effects, it is not possible to maintain a homogeneous strain field throughout a straight test specimen. These difficulties seem to be unavoidable when conventional methods are used.

In 1965, Niordson (Ref. 9) suggested a radically different method, using specimens in the form of thin circular rings. When such a ring expands and rotational symmetry is maintained, the tangential strain is uniform. Furthermore, if the ring is sufficiently thin, the radial stress will be negligible in comparison with the tangential stress, so that the strain field will be approximately unaxial. Finally, there are, of course, no end effects in a ring specimen. With this new method, results have now been obtained for pure copper at strain rates of the order of 2000 sec^{-1} showing a stress-strain relation that features a high initial peak stress for small strains and considerably lower subsequent stresses. It seems most probable that it is these characteristics of the behaviour in the material

that would be distorted when using conventional methods in which the strain field is not homogeneous.

The method described in Ref. (2), which has been used here, requires very accurate measurement of the magnetic force, the radial displacement and the acceleration, since the stress is obtained from the difference between the driving magnetic force and the almost equally large inertia force. It therefore seems to be of interest to describe the devices and techniques used for measuring and computing the stress-strain relation. The main part of this report is devoted to this subject. The material properties at high strain rates found for copper serve to illustrate the results that can be obtained by this method.

II. THE TEST FACILITIES

Fig. 1 shows schematically the arrangement of the test unit. After the capacitor has been charged to a sufficiently high energy level, the ignitron is activated and the capacitor is discharged through the primary coil, which is connected to the energy source by a coaxial cable. The current in the primary coil creates a strong magnetic field which induces a current in the test ring. The resulting magnetic force acts in the radial direction on the ring and deforms it.

Initially, the ring is supported close to the windings of the coil, and the support is designed so that the ring is free to expand. The supporting table is

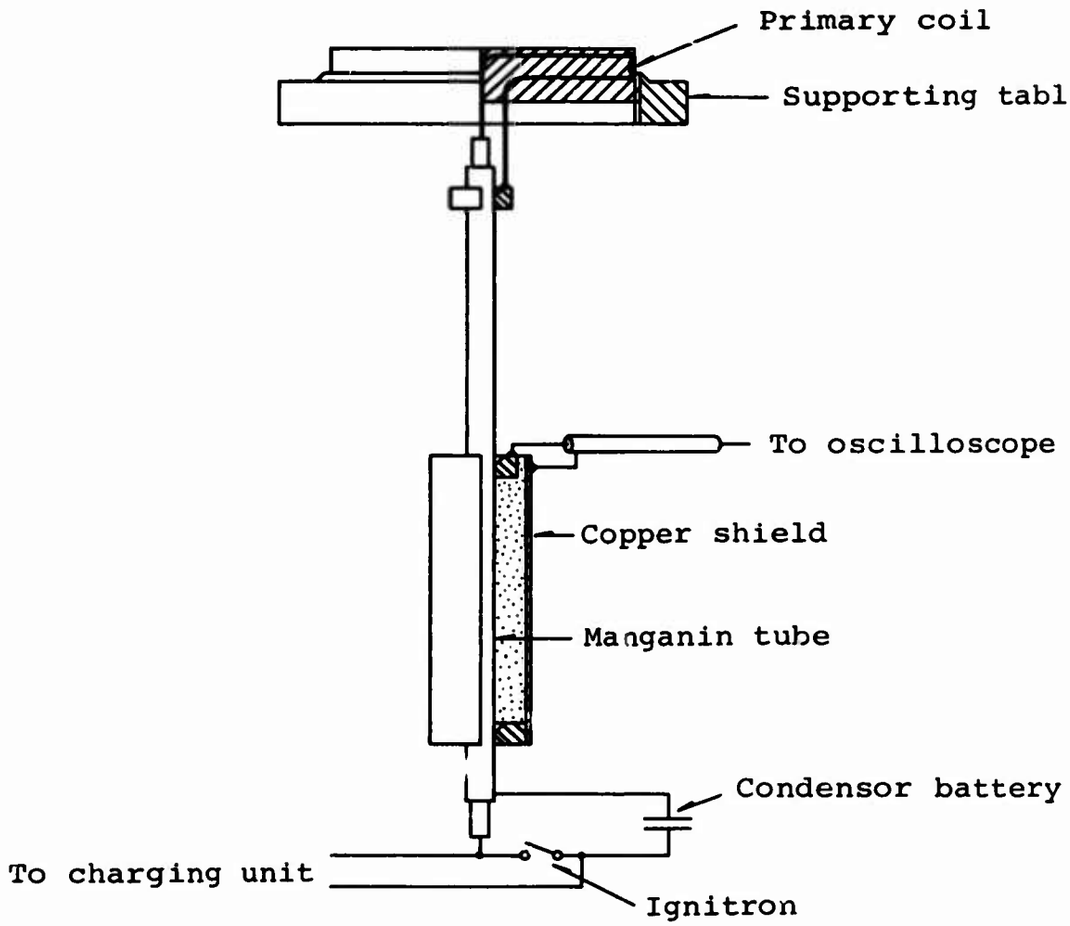

Figure 1 - Principal Arrangement of the Test Unit.

adjustable in the axial direction, accurate adjustment being necessary in order to avoid a resultant vertical force on the ring.

Part of the coaxial cable is made into a shunt, designed for accurate measurement of the primary current. A section of the outer conductor of the cable was replaced by a thin-walled manganine tube which provided effective

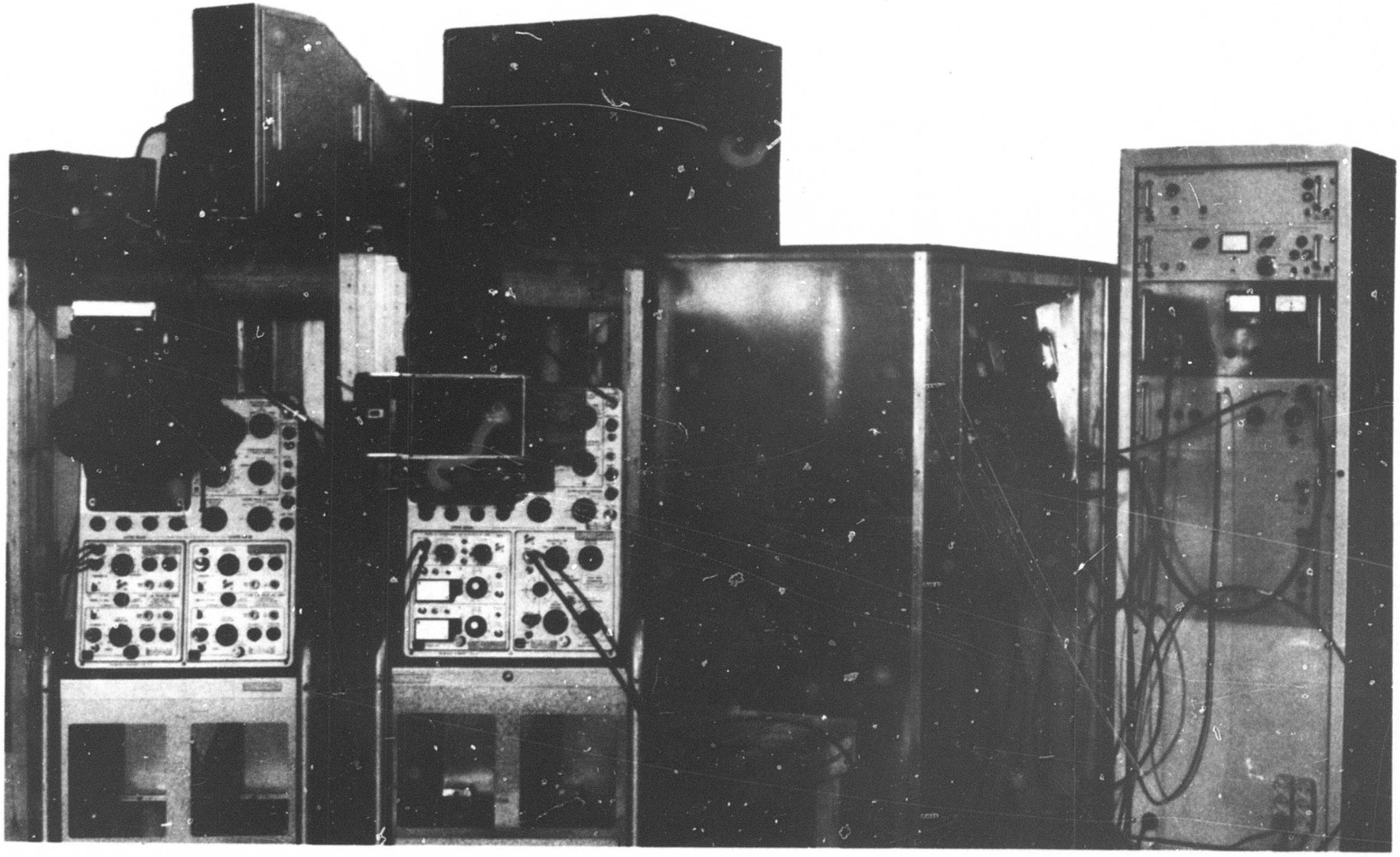

Figure 2 - Facilities for High Strain Rate Testing.

protection against the magnetic field. The voltage across this tube was found to be proportional to the primary current with a high degree of accuracy and was used for obtaining a recording of the current during the test.

Fig. 2 shows how the actual test facilities were arranged during a test. The shielded case in the middle contains the heavy capacitors of in all 32 μF , which are designed for a voltage of max. 25000 V. The controls of the charging unit can be seen on the right-hand side of the case. On top of it is the streak camera (to the left) and a box containing the test specimen. The streak camera is used for a photographic recording of the deformation, i.e. for recording the radial displacement of the ring, which is seen through a narrow slit in the side of the box. The camera is described in some detail below. The box protects the operator and the instruments from pieces of the broken ring, which can easily penetrate half an inch of wood. A flash-lamp (not seen in the photograph) is placed on the opposite side of the box, its light passing through two slits before reaching the streak camera.

The two oscilloscopes seen to the left in the photograph are used for recording the electrical data during the test.

The instruments to the right in the photograph are used for activating the ignitron and the flash-lamp.

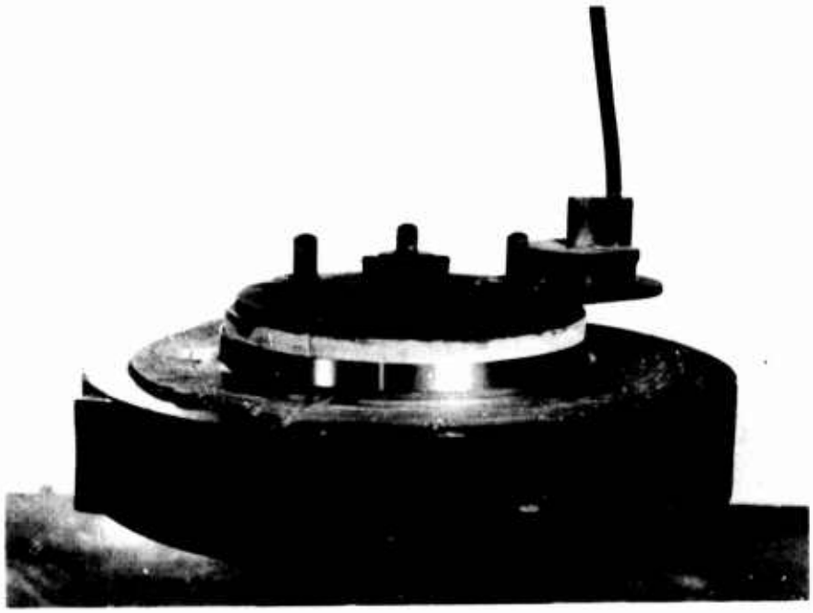

Figure 3 - Primary Coil and Test Specimen.

Fig. 3 shows a close-up of the test ring, the primary coil and the probe (a smaller coil to the right and above the ring), as seen when the protective box is removed. The supporting table and all parts carrying the coils are made of non-metallic materials.

III. THE ENERGY BALANCE

Considering the total energy balance during the time interval dt and taking into account electrostatic, electromagnetic and mechanical energy, we have

$$(1)\quad d\left(\tfrac{1}{2}CV^2\right) + d\left(\tfrac{1}{2}L_1 I_1^{\,2}\right) + d\left(\tfrac{1}{2}L_2 I_2^{\,2}\right) + d\left(L_{12} I_1 I_2\right) +$$

$$+ R_1 I_1^{\,2} dt + R_2 I_2^{\,2} dt + d\left(\tfrac{1}{2}M\left(\tfrac{dr}{dt}\right)^2\right) + 2\pi\sigma A dr = 0$$

where C is the capacity of the condensor battery, and V the voltage across it. I_1 is the current of the coil and I_2 the current of the test specimen. L_1 and L_2 are the instantaneous values of the inductances of the coil and the test specimen, and L_{12} is the instantaneous value of the mutual inductance between the two circuits. The terms $R_1 I_1^2$ and $R_2 I_2^2$ account for the electric losses due to the electric resistances R_1 and R_2 of the primary circuit and the test specimen, respectively, and the term $d(\frac{1}{2}M(\frac{dr}{dt})^2)$ represents the increase in kinetic energy of the ring, where M is its total mass and dr/dt its radial velocity. Finally, the term $2\pi\sigma A dr$ is the work done by the internal forces on the ring during the displacement dr .

For the primary circuit we have

$$V + R_1 I_1 + \frac{d}{dt}(L_1 I_1) + \frac{d}{dt}(L_{12} I_2) = 0 \tag{2}$$

and

$$C \frac{dV}{dt} = I_1 \tag{3}$$

It is possible to eliminate the resistance R_1 and the voltage V between the equations (1), (2) and (3) . Similarly, for the secondary circuit i.e. the test specimen, we get

$$R_2 I_2 + \frac{d}{dt}(L_2 I_2) + \frac{d}{dt}(L_{12} I_1) = 0 \tag{4}$$

The resistance R_2 of the test specimen may now be eliminated and the resulting equation reads

$$(5) \quad -\frac{1}{2} I_2 \frac{dL_2}{dr} \frac{dr}{dt} - I_1 I_2 \frac{dL_{12}}{dr} \frac{dr}{dt} + M \frac{dr}{dt} \frac{d^2r}{dt^2} + 2\pi\sigma A \frac{dr}{dt} = 0$$

or

$$(6) \quad \sigma = \frac{1}{2\pi A} I_1 I_2 \frac{dL_{12}}{dr} + \frac{1}{2\pi A} I_2^2 \frac{dL_2}{dr} - \frac{M}{2\pi A} \frac{d^2r}{dt^2}$$

Due to the short duration of the high strain rate tensile test, the acceleration and hence also the inertia forces are of considerable magnitude. In most cases, the stress in equation (6) is actually obtained as a comparatively small difference between the sum of the first two terms, representing the stress due to the electromagnetic forces, and the last term, which accounts for the inertia. Thus, to obtain the stress with even a moderate degree of accuracy, all terms in equation (6) have to be determined with very high accuracy.

IV. DEFORMATION ANALYSIS

A series of tests using the open-shutter technique described in Ref. (1) has shown that the test ring maintains a rotational symmetry and that it expands coaxially

during its deformation. This behaviour is, of course, due to the self-centering and stabilizing properties of the magnetic field. Hence, the measurement of the deformation is reduced to finding the radius $r(t)$ of the ring as a function of time. The strain, strain rate and inertia forces are determined from this function. However, this requires that the acceleration, represented by the second derivative d^2r/dt^2, can be computed with sufficient accuracy. This is no doubt, one of the main difficulties encountered. Several different methods have been used for measuring the radial deformation. One seemingly promising method involved a photo multiplier to measure the light intensity of a region containing the shadow of the ring. This method permitted the derivatives dr/dt and d^2r/dt to be obtained using operational amplifiers. However, in the end the method had to be discarded as not being sufficiently accurate. The method finally employed involves the use of a streak camera.

A schematic view of the streak camera is shown in Fig. 4. The optical axis of the camera is tangent to the test ring A, and the objective focuses the edge of the ring into the slit C. The slit, which is partly covered by the image of the ring, is projected onto the film plane G by means of the objective D, the beam splitter E and the rotating mirrors F. With a light behind the ring, this arrangement results in a thin line of light on the film plane parallel to the axis of the rotating mirrors. As the ring expands, the shadow of the

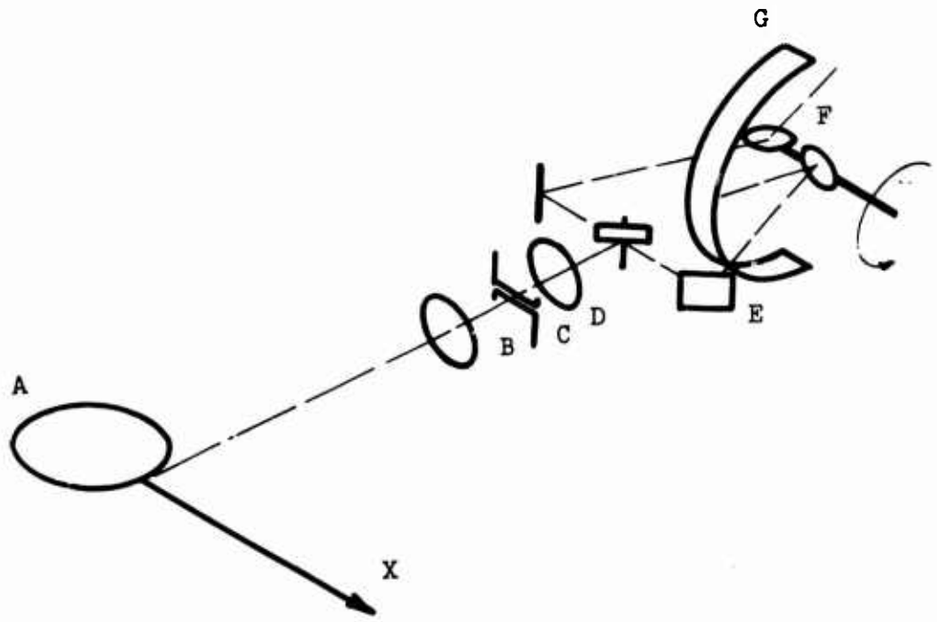

Figure 4 - Principal Arrangement of the Streak Camera.

ring gradually covers the slit and the length of the line on the film plane diminishes. The length of this line gives a very accurate measurement of the radial deformation of the ring.

When the mirrors F rotate at constant speed and the ring expands, a continuous curve is recorded on the film, yielding the radial motion of the ring as a function of time. Fig. 5 shows a typical recording at 25800 rpm.

It is comparatively easy to calibrate the streak

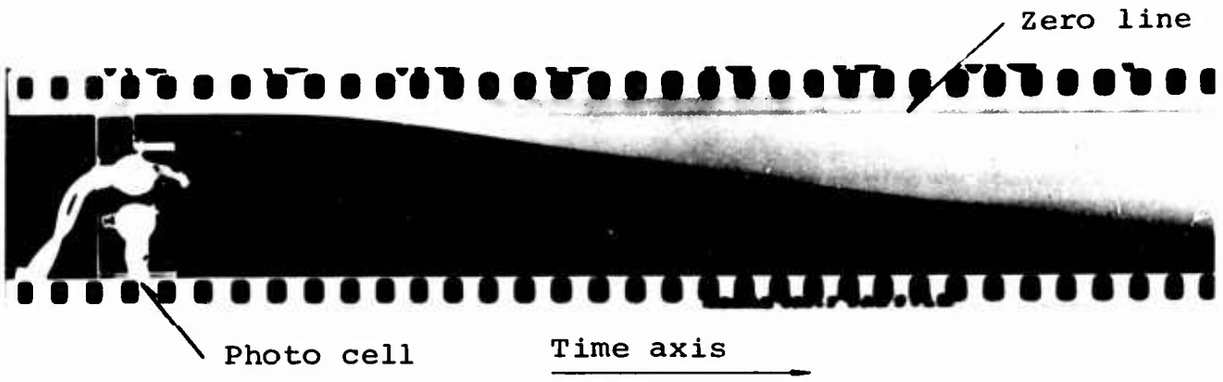

Figure 5 - Streak Recording.

camera accurately. By placing a scale at the focal plane and photographing it, an accurate calibration of the radial deflection coordinate is obtained.

The time scale is determined from the streak velocity of the camera. Due to the finite thickness 2ℓ of the mirrors, the streak velocity v is not simply $2\omega\rho$, (where ρ is the radius of the film plane) but can be shown to be

$$(7) \qquad v = 2\omega\rho \, \frac{2(a\cos\phi+\ell)^2 - a\cdot c\cdot\cos 2\phi - \ell\cdot c\cdot\cos\phi}{(c-2(c-a)\cos^2\phi + 2\cdot\ell\cdot\cos\phi)^2}$$

where the corretive factor is a function of ϕ (the angle of the mirrors as a function of time). The constants a and c depend upon the geometry of the camera. In the case in question we have $\rho = 160.00$ mm , $\ell = 2.85$ mm , $a = 145.85$ mm , and $c = 147.48$ mm .

Referring to Fig. 5, the zero-line shown is obtained by a separate exposure and the photo cell seen to the left is used for synchronizing the streak recording and the electrical recordings.

The angular velocity ω is determined as the mean value during a certain period of time, using an automatic electronic counter activated by a magnetic pick-up applied to the shaft of the mirrors.

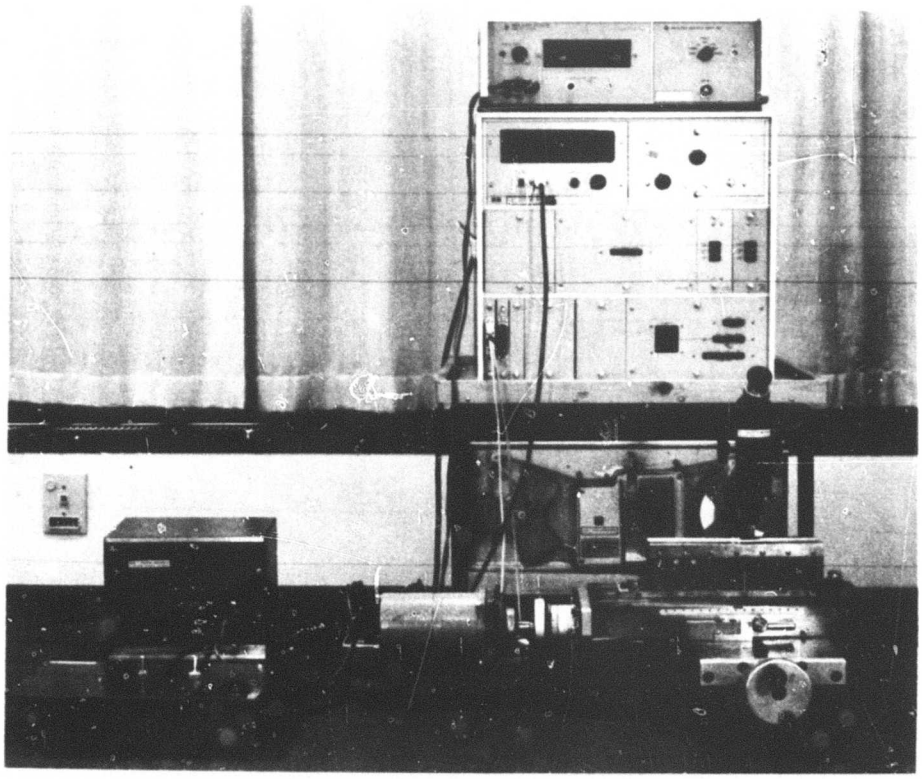

Figure 6 - Facilities for the Analysis of Recordings.

Fig. 6 shows the facilities for analyzing the streak recording. A step motor is connected to a solid x-y-table equipped with a microscope. When activated, the step motor moves the table in the x-direction a step of 0.50 mm (roughly corresponding to 0.8 μsec. of the time-axis of the recording in Fig. 5). A differential transformer is connected to the table in such a manner that the displacement in the y-direction results in a voltage proportional to it. The voltage is measured by a digital voltmeter, the output of which is punched on paper tape.

Using the zero-line (Fig. 5), the recording is aligned parallel to the x-axis of the table and the analysis can proceed step by step, resulting in a series of data punched on tape. A photo of the calibration scale is analyzed immediately after the streak recording, yielding the scale factor for the radial displacement.

The analysis of the recording (Fig. 5) can now be performed with a high degree of accuracy, yielding the radial displacement r as a function of time t .

V. MAGNETIC FORCE ANALYSIS

In this section the procedure involved in determining the magnetic force represented by the first two terms of equation (6) is described.

The determination involves separate measurements of the primary and secondary currents I_1 , and I_2 ,

respectively, and of the derivative dL_{12}/dr . The derivative dL_2/dr , which is also involved in equation (6), is not determined experimentally but rather by

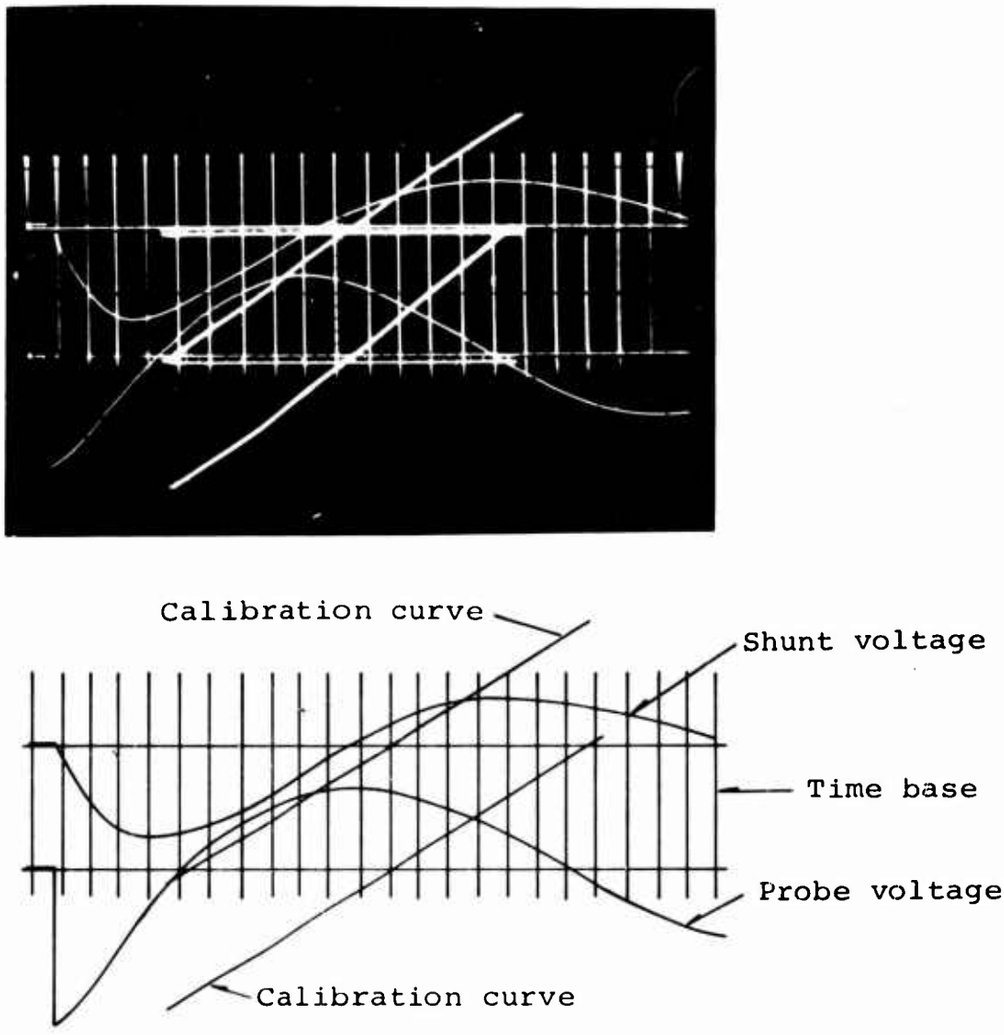

Figure 7 - Oscilloscope Recordings.

using the theoretical expression for the self-inductance of a short, thin-walled cylinder

$$L_2 = 4\pi R\left(\ell n\left(\frac{8R}{h}\right) - \frac{7}{4}\right)\cdot 10^{-7} \quad (H) \tag{8}$$

where R is the mean diameter and h the thickness. Differentiation with respect to R yields:

$$\frac{dL_2}{dR} = 4\pi\left(\ell n\left(\frac{8R}{h}\right) - \frac{3}{4}\right)\cdot 10^{-7} \quad (H/m) \tag{9}$$

The currents I_1 and I_2 are determined from oscilloscope recordings. Fig. 7 shows a typical recording of the shunt voltage (proportional to I_1), the probe voltage V_3 (from which I_2 is determined), and the necessary calibration curves together with the time base.

As the inductance of the shunt was found to be negligible, there is no phase shift between the primary current I_1 and the voltage V_1 across the shunt. Thus

$$I_1 = \frac{V_1}{R_s} \tag{10}$$

where R_s is the resistance of the shunt. This resistance was determined as an average of 10 measurements (Fig. 8).

It was found that

$$R_s = 2.285\cdot 10^{-3}\ \Omega$$

at a frequency of 5 kc, which corresponds to test conditions. It should be noted that at DC conditions,

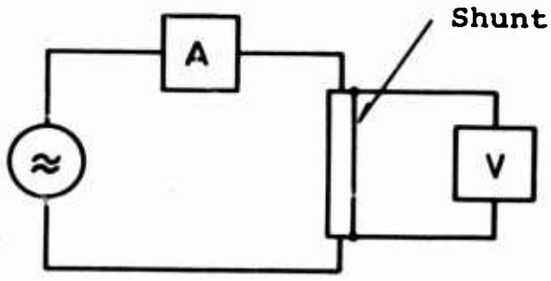

Figure 8 - Determination of Shunt Resistance.

the resistance of the shunt was found to be $2.279 \cdot 10^{-3}\ \Omega$, i.e. slightly lower, but the difference is below the threshold of accuracy and we may conclude that the inductance of the shunt is negligible. This can definitely be attributed to its coaxial design.

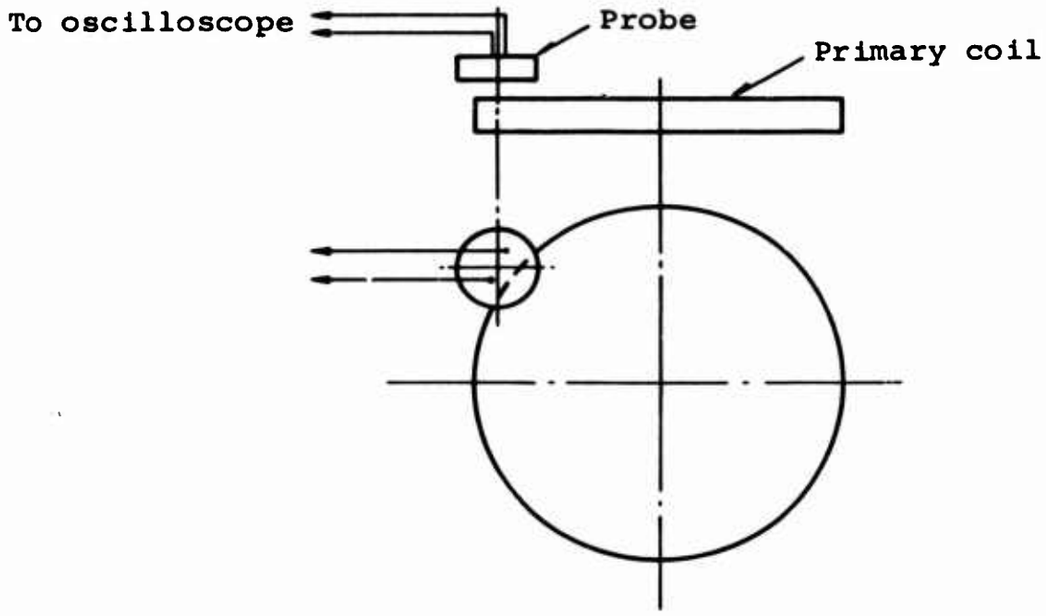

Figure 9 - Principal Arrangement of the Probe.

Fig. 9 shows schematically the arrangement of the probe used to determine the secondary current I_2 .

Let L_{13} be the mutual inductance between the probe and the primary coil, and L_{23} the inductance between the probe and the test specimen. Then the voltage V_3 induced in the probe will be

$$V_3 = \frac{d}{dt}(L_{13}I_1) + \frac{d}{dt}(L_{23}I_2) \tag{11}$$

The resistance of the probe is negligible in comparison with the input impedance of the oscilloscope so V_3 is the voltage on it.

As the probe is fixed relative to the primary coil, L_{13} is constant, and the current I_2 is found from equation (11) to be

$$I_2 = \frac{1}{L_{23}} \int_0^t V_3 dt - \frac{L_{13}}{L_{23}} I_1 \tag{12}$$

The position of the probe is always adjusted radially so that L_{13} becomes as small as possible. This reduces the influence of I_1 on the result (Eq. 12). The probe then mainly measures the secondary current I_2 .

It was found necessary to calibrate the oscilloscope before each test. The time base was indicated using a differentiated 100 kc square wave signal supplied from the internal oscillator of an electronic counter. Thus the vertical lines of Fig. 7 are spaced at intervals of 10 μsec.

Careful checking of several recordings showed that the time base of the oscilloscope was linear except at the very ends of the display.

We used this result for calibrating the vertical gain of the oscilloscope in the following manner. A sinusoidal wave signal was applied to the vertical and the horizontal inputs of the instrument. The resulting calibration curves (one for each channel), which deviate slightly from straight lines, are thus obtained, and these are used for evaluating the ordinates of the voltage curves.

The mutual inductance L_{12} between the primary coil and the test specimen was determined using a set of 10 copper rings of different radii ranging from 140 mm to 186 mm. These rings were made in such a way that the cross-sectional dimensions were in inverse proportion to the square root of the radius so that the volume (or mass) was the same for all rings. The set could represent the expanding test ring at different stages. Each ring was cut and connected to a differential voltmeter according to Fig. 10.

The voltage E measured is proportional to the current I introduced in the primary coil, the factor of proportionality being ωL_{12}. Thus we have

$$L_{12} = \frac{E}{I\omega} \tag{13}$$

where ω is the angular frequency of the current. We used a frequency of 5 kc, which corresponds roughly to the actual test conditions.

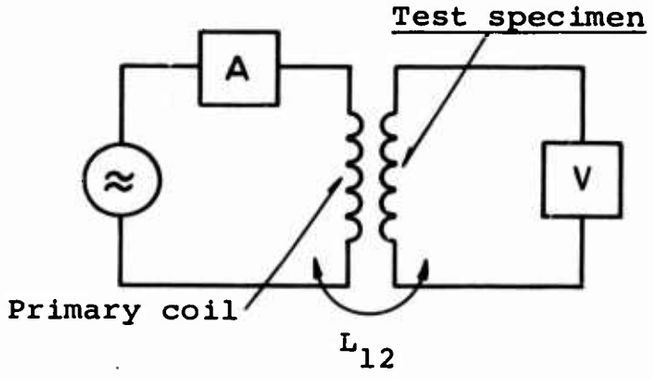

Figure 10 - Arrangement During Measurement of the Mutual Inductance L_{12}

The result of the measurement (used in the analysis of tests 44-48) is given in the appendix, table 1. Approximating L_{12} by a polynomial of 2nd degree, we obtain

$$L_{12} = a_1 + b_1 R + c_1 R^2 \tag{14}$$

where the coefficients a_1, b_1, and c_1 were determined by the method of least squares from the measured values of L_{12} and R. From this formula we obtain

$$dL_{12}/dr = b_1 + 2c_1 R \tag{15}$$

which is used in Eq. (6).

Clearly, in order to obtain I_2 we must know L_{13} and L_{23}. The mutual inductance L_{13} between the primary coil and the probe was determined as an average of 10

measurements. We found that

$$L_{13} = 0.513 \quad \text{nH}$$

which, as we shall see, is considerably less than the values obtained for L_{23} .

The mutual inductance L_{23} between the test ring and the probe is determined in much the same way as L_{12} ,

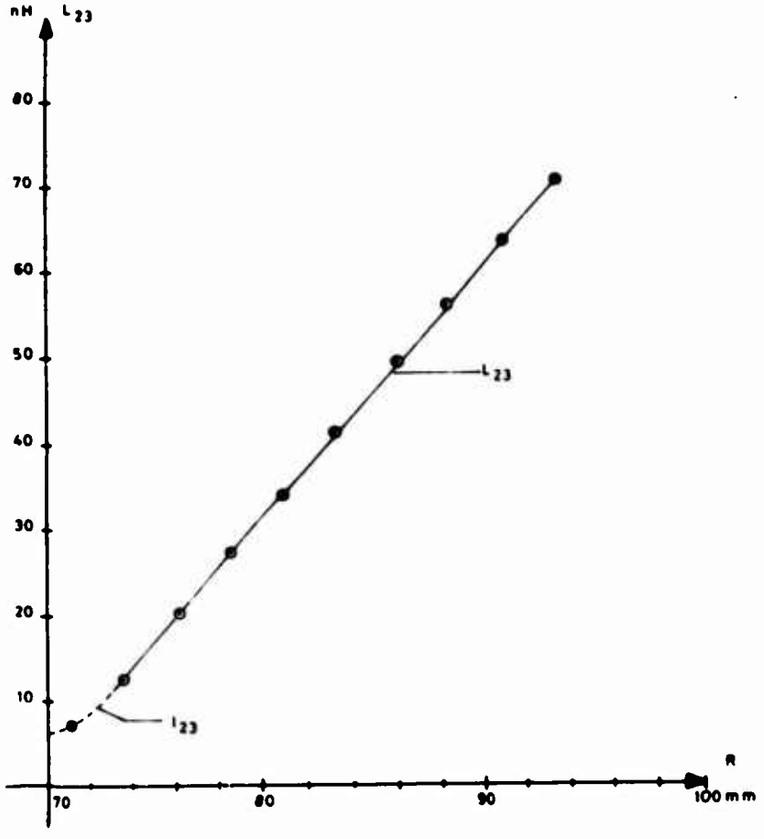

Figure 11 - The Mutual Inductance L_{23} .

using the same set of rings. Fig. 11 shows the inductance L_{23} as a function of R_1 . The values obtained in the measurements are reported in the appendix, table 2.

In order to have an accurate representation of the function $L_{23}(R)$, we found it convenient to sub-divide the range of R into two parts in the following manner

$$(16)\quad L_{23} = \begin{cases} a_2 + b_2 R + c_2 R^2 & \text{for} \quad R \leq 73.5 \text{ mm} \\ a_3 + b_3 R + c_3 R^2 & \text{for} \quad R \geq 73.5 \text{ mm} \end{cases}$$

where the coefficients $a_2, \ldots, c_3$ are determined by the least squares method and such that L_{23} and dL_{23}/dR are continuous at $R = 73.5$ mm .

With L_{23} , we now have all that is required to determine the secondary current I_2 from Eq. (12).

In order to determine the magnetic forces according to Eq. (6) , we must have all quantities I_1 , I_2 dL_{12}/dr , and dL_2/dr as functions of time t . The last two are known to us now as functions of the radial displacement r . We know r as a function of time, but we must establish <u>simultaneous</u> values of the quantities mentioned.

Further, in order to find simultaneous values of the magnetic forces and the inertia forces, we must correlate the time axes of the streak recording and the oscilloscope recordings accurately. The synchronization presented one of the main problems and is discussed in the next section.

VI. SYNCHRONIZATION

When the actual test is performed the operator starts a series of processes when he presses the button. Assuming that the capacitors are charged and that the mirrors of the streak camera rotate at their operating speed, the starting impulse must initiate the flash, the ignitron and the oscilloscope. Preferably, the ignitron should be activated when the mirrors are in a favourable position and this is why we let the light reflected by the mirror initiate the ignitron (and the oscilloscope) when it hits a photo diode placed suitably in the film plane (see Fig. 5). The active part of this photo diode measures only 0.5 mm in cross section and the zero position on the film plane is thus well defined. The whole process is therefore started by the operator switching on the flash lamp. The light reflected by the rotating mirrors sweeps the film plane and when it reaches the photo diode (t=0) this is activated and the pulse starts the other processes.

Fig. 12 is an outline of the ignitron system. When the photo diode is illuminated by the ray from the flash, a pulse is transmitted through the amplifiers 1 and 2 activating the ignitron. A fraction of the pulse from amplifier 1 is used to trigger the oscilloscope. Throughout this system the pulse is delayed and we denote by

ΔT_1	the	time	delay	of	the photo diode
ΔT_2	"	"	"	"	amplifier 1
ΔT_3	"	"	"	"	amplifier 2 + ignitron
ΔT_4	"	"	"	"	the oscilloscopes

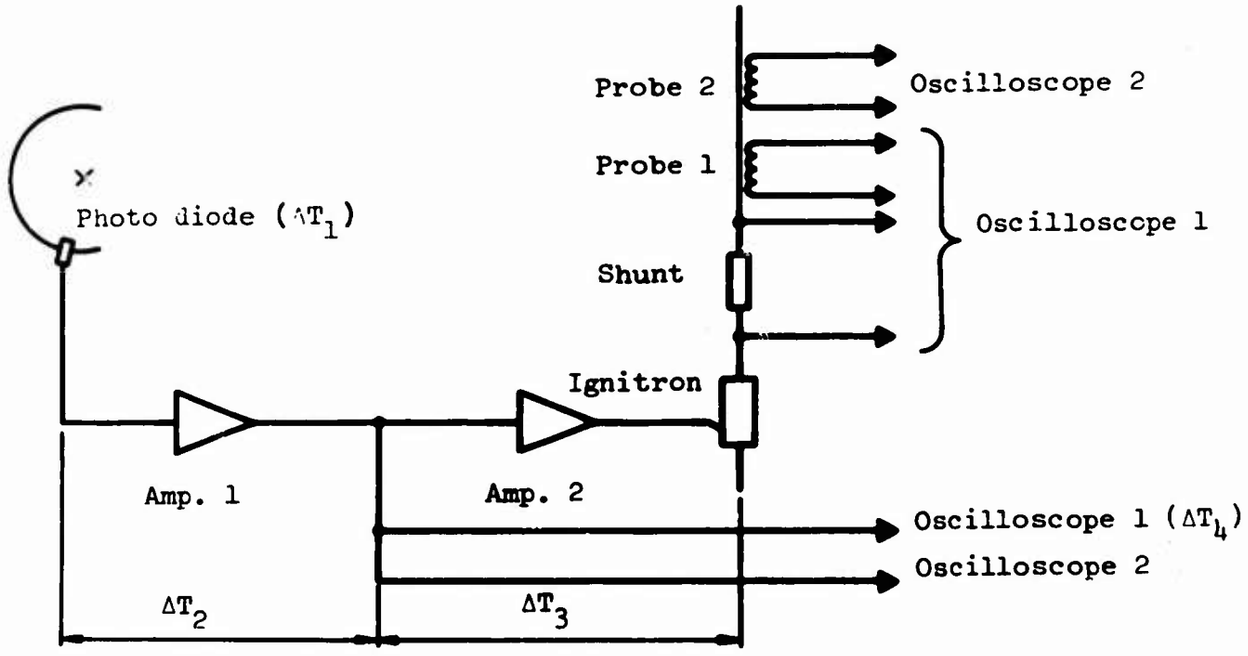

Figure 12 - The Ignitron System.

These time delays should be added according to the scheme in Fig. 12.

The photo diode is a so-called pin diode with a rise time of only about 1 nsec , which is completely negligible in comparison with the time scale of the test (order of magnitude: 100 μsec) . The same applies to the oscilloscope, which have a rise time of about 10 nsec . Thus, for our purpose, we may put $\Delta T_1 = \Delta T_4 = 0$.

The time delay ΔT_2 of amplifier 1 was determined electrically using a single-pulse input. It was found that this interval was independent of the input voltage and of the triggering level of the oscilloscope.

We found

$$\Delta T_2 = 0.92 \ \mu sec$$

In order to determine ΔT_3 we connected the vertical amplifier of a second oscilloscope (2) to a small probe (indicated as "Probe 2" in Fig. 12), which was wound around the connection to the primary coil. The sweep of oscilloscope 2 is triggered by amplifier 1 and the primary current induces a voltage in the probe, which is registered as a sharp peak on the trace. By choosing a suitable sweep velocity (2 μsec/cm), the time delay ΔT_3 was obtained with a high degree of accuracy as corresponding to the horizontal length of the trace up to the peak. It was found that ΔT_3 was different in each test, varying between 5 and 25 μsec . This is certainly due to the ignitron.

Before analyzing a streak recording, the time delay ΔT_3 of each individual test is determined and the total time delay ΔT is then found from

$$\Delta T = \Delta T_3 + 0.92 \ \mu sec$$

The circuits of the pulse amplifiers 1 and 2 are shown in Figs. 13 and 14 respectively. In Fig. 14, V_4 is a high voltage thyratron, which activates the ignitron V_5 through a pulse transformer T_6 .

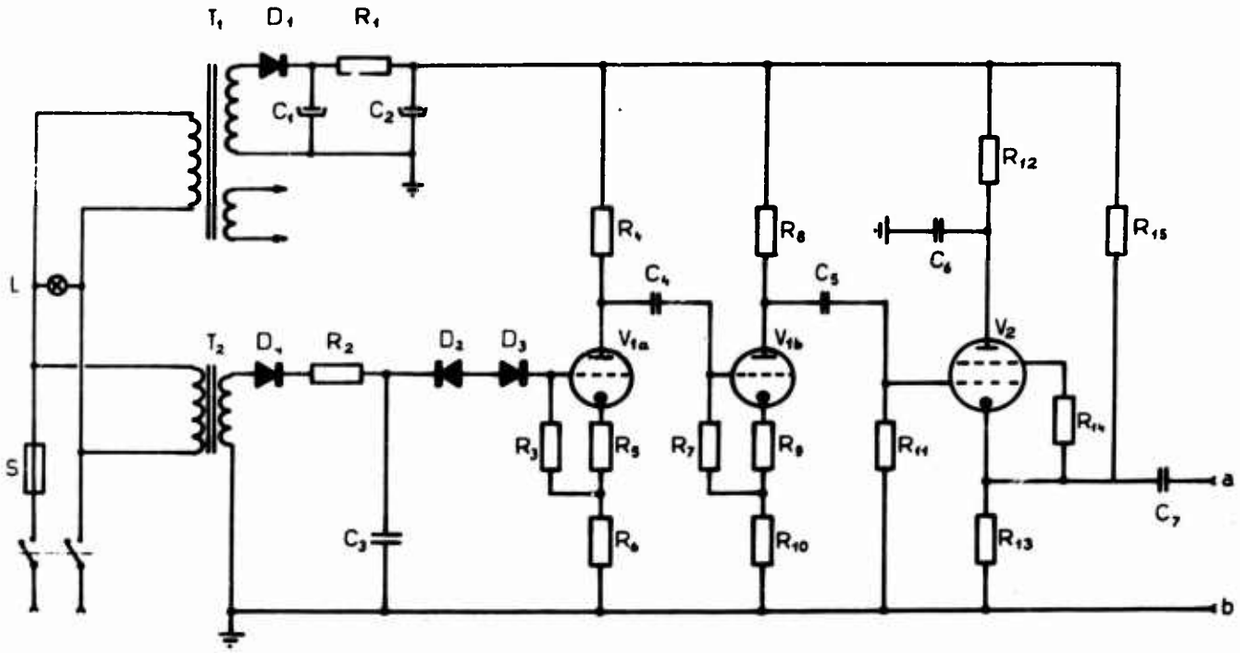

Figure 13 - Pulse Amplifier 1.

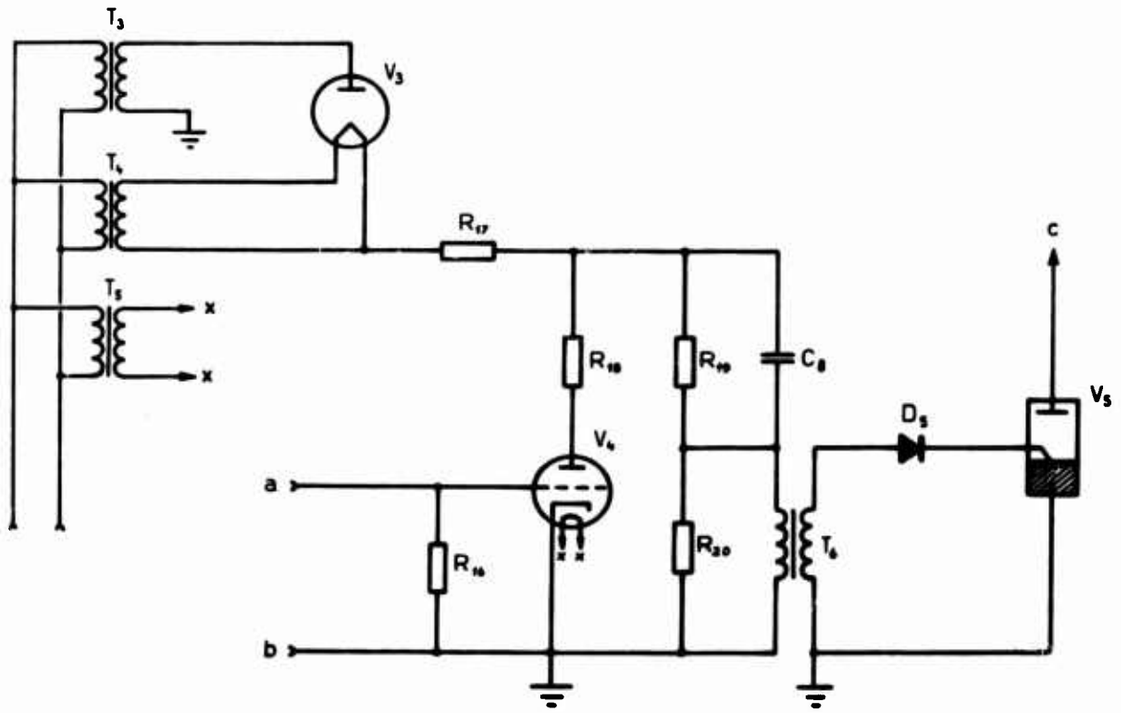

Figure 14 - Power Amplifier 2.

VII. TEST PROCEDURE

The successful analysis of any test depends upon an accurate determination of the mutual inductances L_{12} , L_{13} , and L_{23} . Whenever a new series of tests is carried out after any operation (or break down) that might have changed these inductances, they have to be determined again according to the procedures described above. The vertical position of the test ring is critical for a successful test. Special precautions are necessary to ensure that the magnetic forces have no appreciable vertical component on the ring. The support of the ring is therefore carefully adjusted in a vertical position before the test. However, the vertical position of the ring has a considerable influence on the mutual inductance L_{23} and it is therefore necessary to measure L_{23} after any adjustment of the vertical position. For practical reasons, such adjustment is then performed before a series of tests with identical specimens.

In Fig. 1 it will be seen that the supporting table has a circular wedge. This has the same diameter as the test ring and supports it before the test. The support can be adjusted vertically and its correct position is found using the device shown in Fig. 15. This consists of two copper rings of the same thickness and diameter as the test ring. They are, however, much narrower that the test specimen and are fixed in position by a bakelite ring in such a manner that the total height of the device is equal to the height of the test ring. Each ring was cut and the ends were connected to a differential voltmeter.

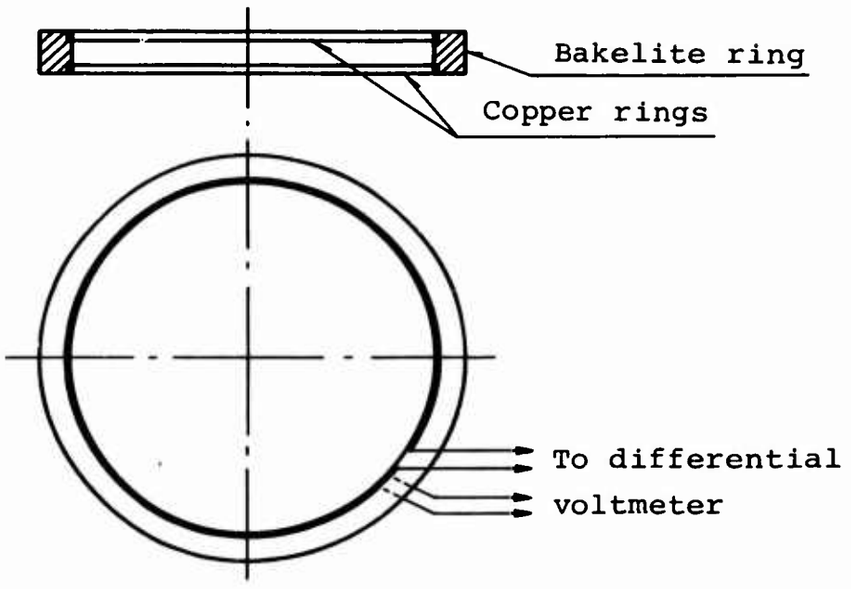

Figure 15 - Arrangement for Vertical Adjustment.

By applying an AC current to the primary coil, the device was adjusted vertically until the voltages induced in both rings were exactly equal. In this position, there is no vertical force on the test ring, and the supporting table was therefore locked at this height.

In order to investigate the vertical adjustment, several tests were carried out at a 5 kV charge. At this energy level the rings did not fracture but expanded considerably. After the test they were examined and found to have deformed in perfect symmetry. It should be noted that an inaccurate adjustment invariably resulted in the rings deforming into cones.

Before each individual test the ring was measured carefully. It was then covered with soot on the outside and weighed. The soot was applied in order to avoid

undesirable reflexions from the flash light.

The oscilloscope was now calibrated, i.e. the calibration curves and the time base shown in Fig. 7 were exposed into the recording. The capacitors were charged to a voltage slightly above the energy level at which the test was to be performed. The voltage was indicated by a digital voltmeter, which was applied to a voltage divider connected directly to the capacitors. After disconnection of the charging unit, the voltage would slowly fall. The streak camera was started and when the voltage reached the exact energy level for the test, the flash lamp was switched on and the test was started and recorded.

VIII. TEST RESULTS

In developing the equipment and the measuring technique, a great number of specimens of aluminum, zink and steel, but mainly of copper were tested. Over 150 copper rings were tested to fracture. The results of 52 tests were analyzed. During the tests several errors were corrected and the procedure was improved. In this final report we present the results of the last nine tests on commercially available pure copper in its original and in annealed condition. These results are presented here as an illustration of the possibilities of the test method rather than from an interest in the material itself.

Tests Nos. 44-48 (Series I) were conducted on pure copper in its original state (as commercially available)

and tests Nos. 49-52 (Series II) on annealed copper. The rings were annealed in neutral atmosphere at 600°C for 5 hours. All specimens of both series had the same nominal size, i.e. outer diameter 142 mm, thickness 1 mm and height 10 mm. The mass was about 0.039 kg per ring.

The tests of both series were performed at an energy level of 10 kV. The different tests of each series were made in order to investigate if and how closely they could be reproduced and only one parameter (the condition of the material) varied between the series.

Series I

The results of tests 44-48 are given in the graphs on pages 30-34. In the mean, the (maximum) strain rate was 1836 sec^{-1} and varied within only about 5 per cent. All specimens fractured in small pieces.

The stress-strain relation at this high strain rate can be deduced from the graphs. We find a linear range for strains below 0.5 per cent and a high peak yield stress varying from about 700 N/mm^2 to about 1200 N/mm^2. At about 4 per cent strain the stress falls considerably to the order of 200 N/mm^2 and then rises slowly in the range shown of 12 per cent strain.

The peak stress at about 1 per cent strain is roughly 3 times the yield stress of the material measured at low strain rates.

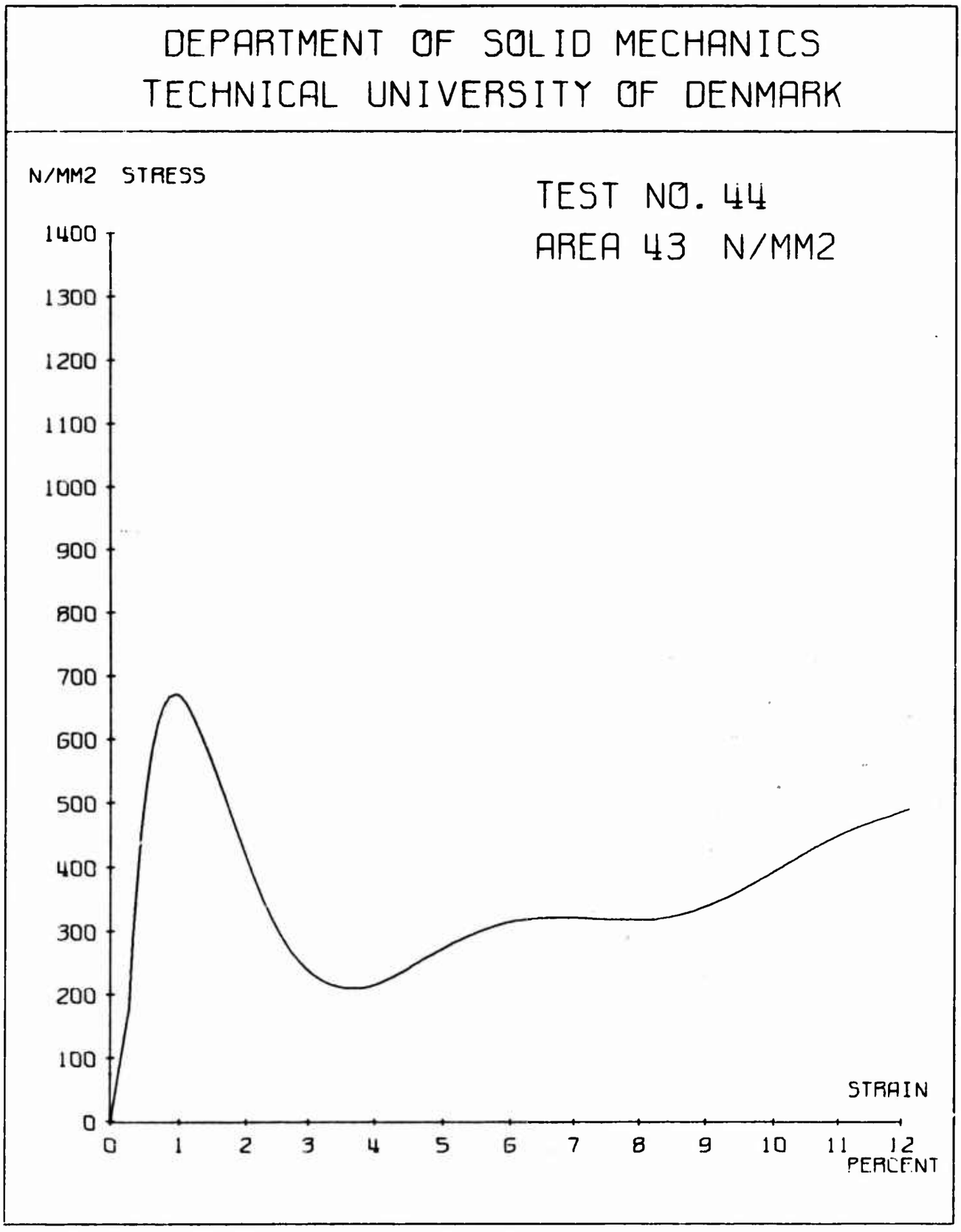

Fig. 16 - Stress-Strain Curve, Test No. 44

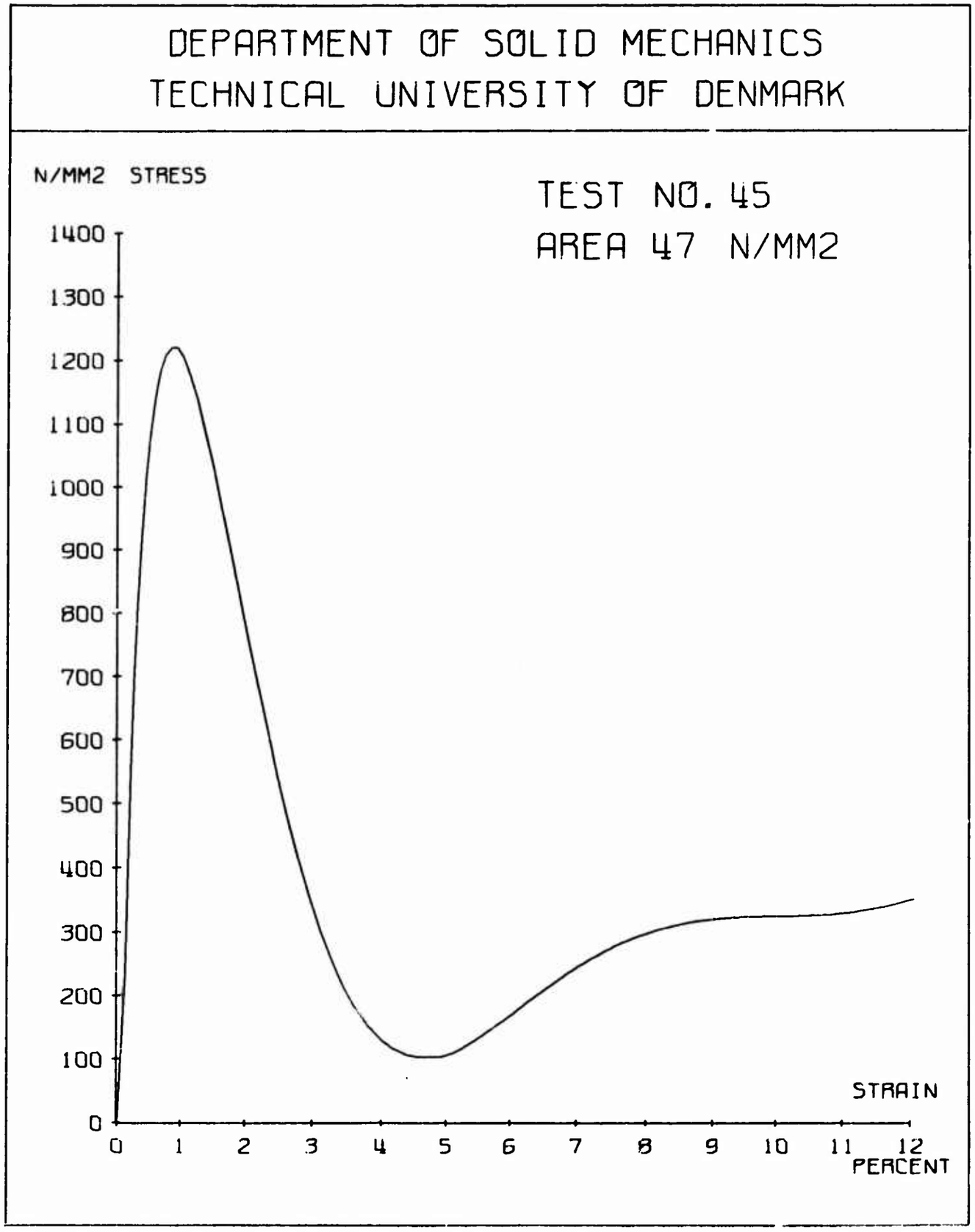

Fig. 17 - Stress-Strain Curve, Test No. 45

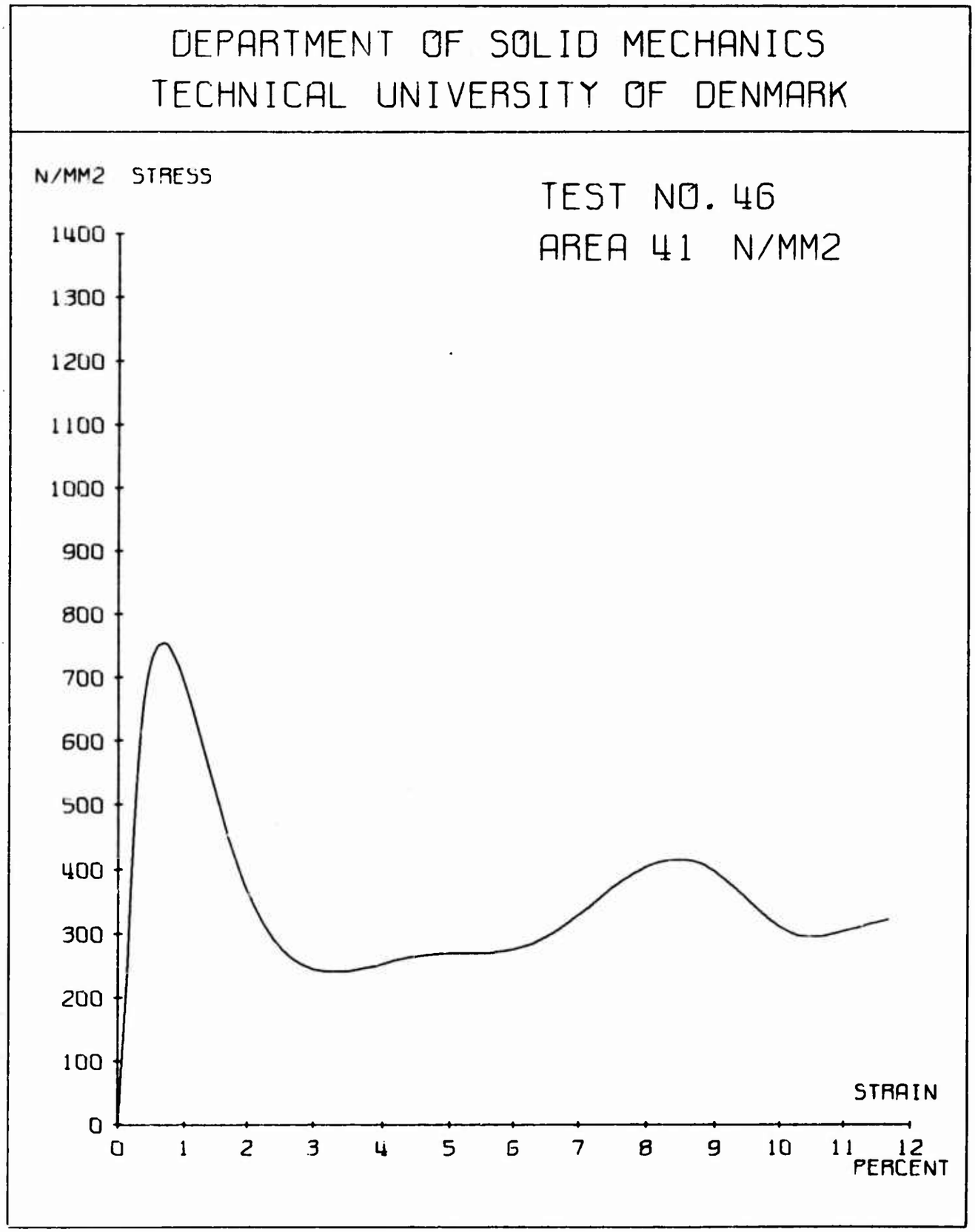

Fig. 18 - Stress-Strain Curve, Test No. 46

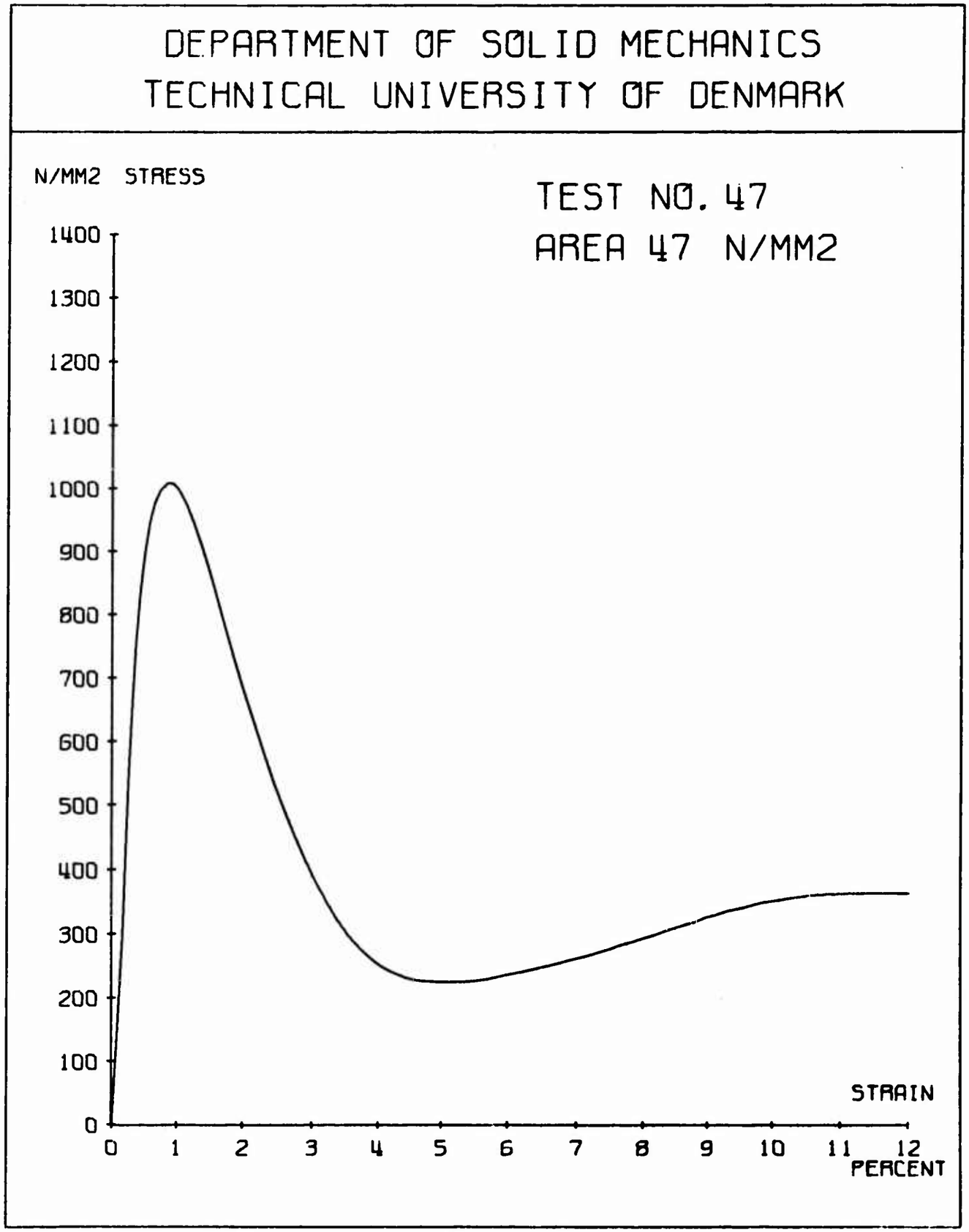

Fig. 19 - Stress-Strain Curve, Test No. 47

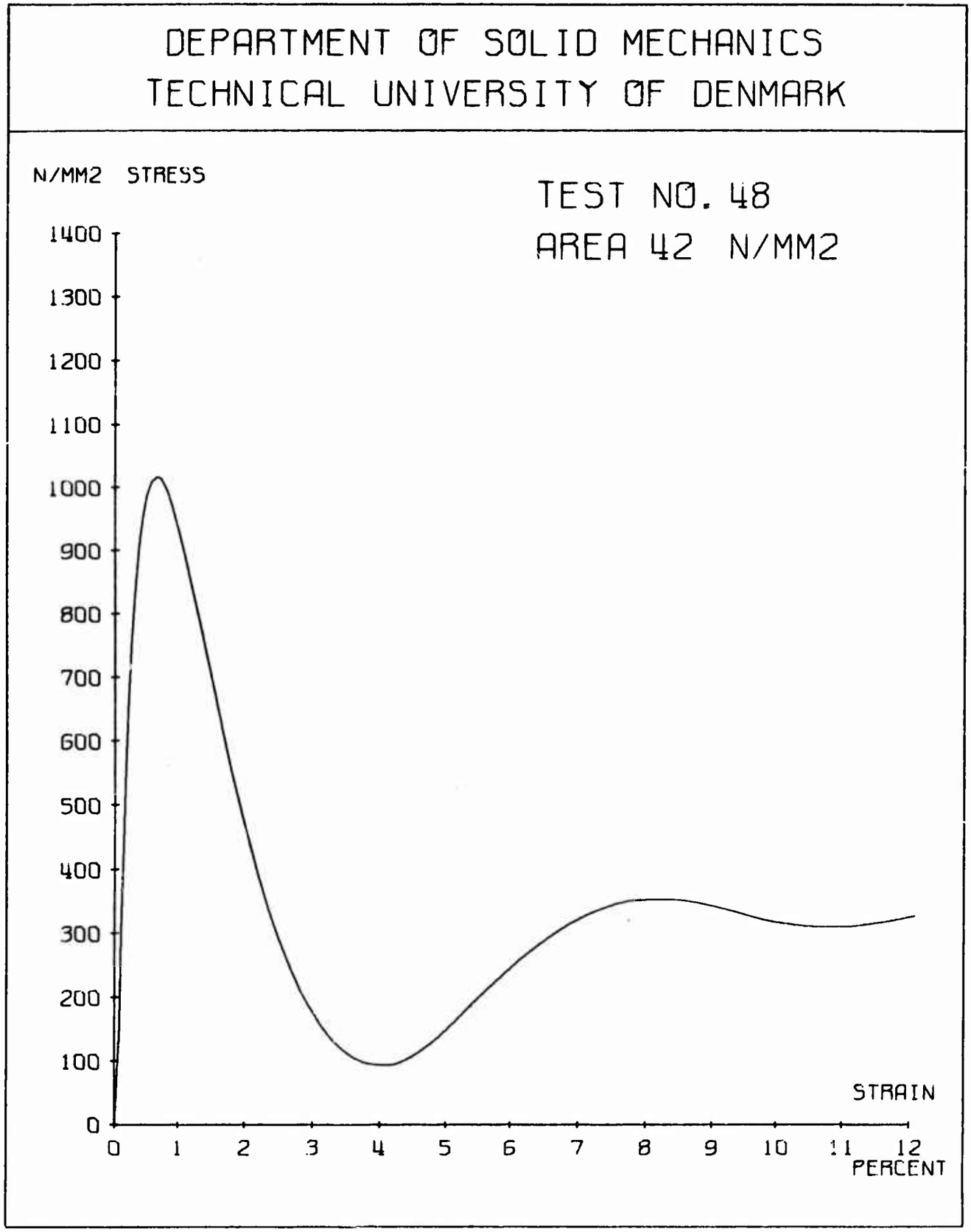

Fig. 20 - Stress-Strain Curve, Test No. 48

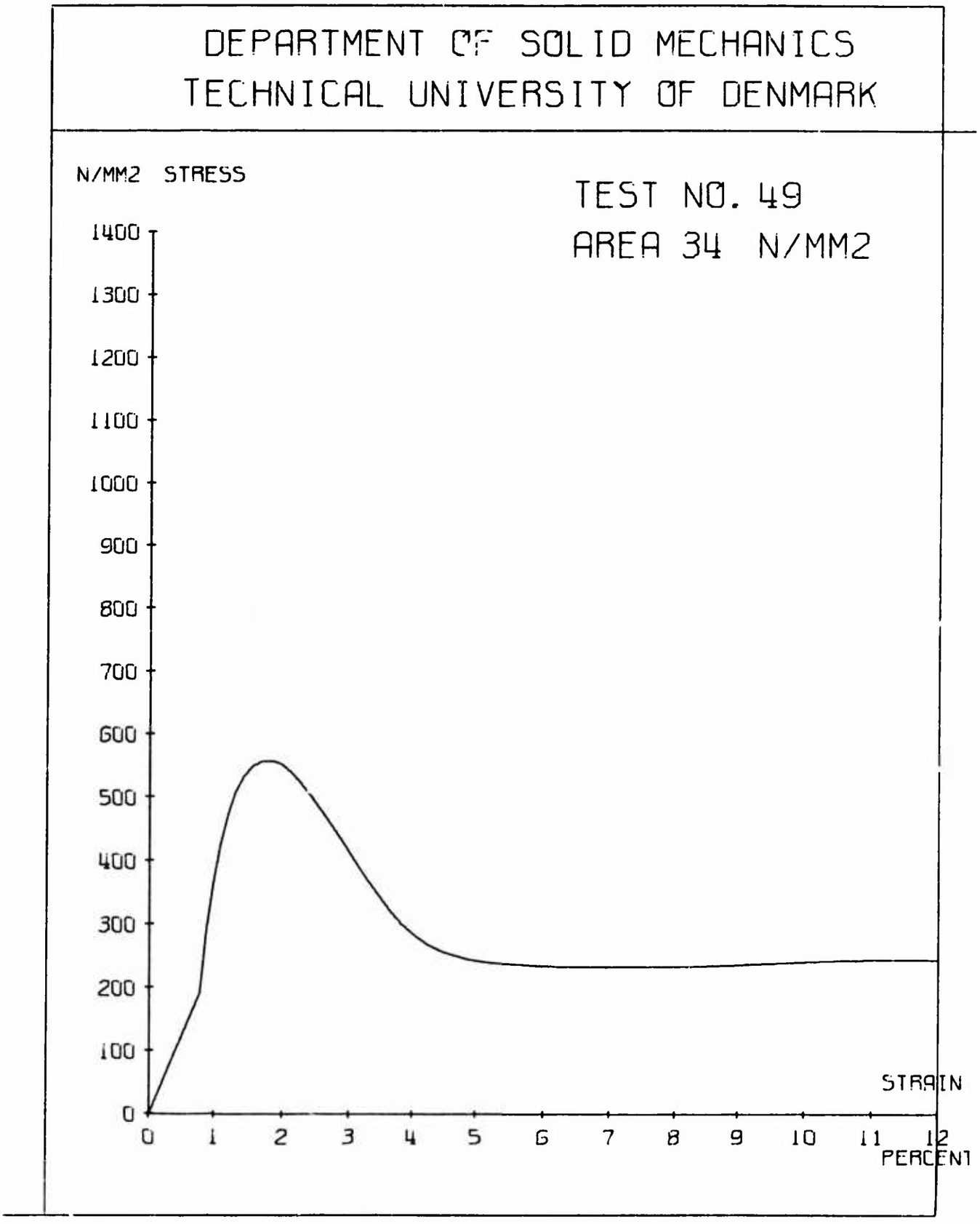

Fig. 21 - Stress-Strain Curve, Test No. 49

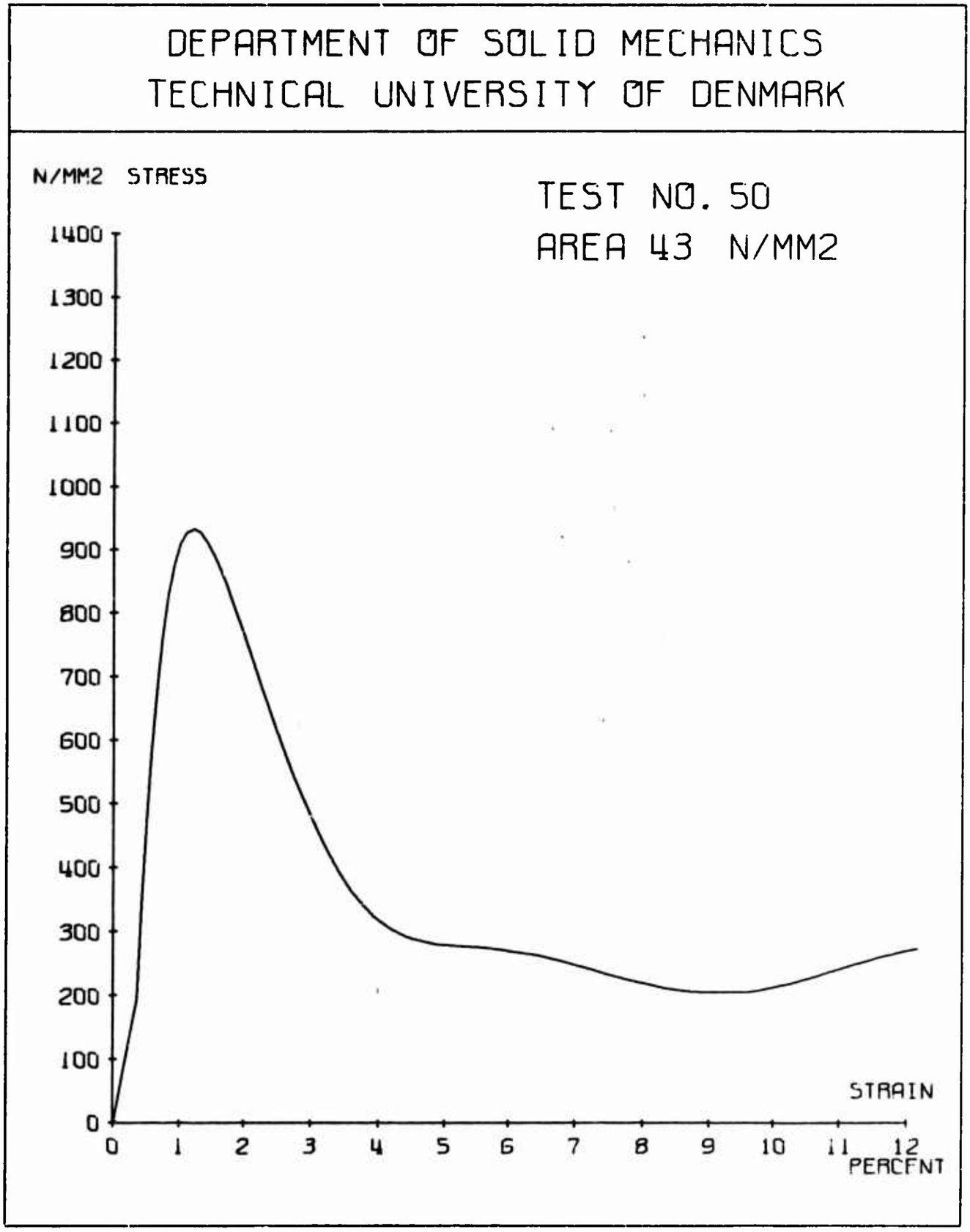

Fig. 22 - Stress-Strain Curve, Test No. 50

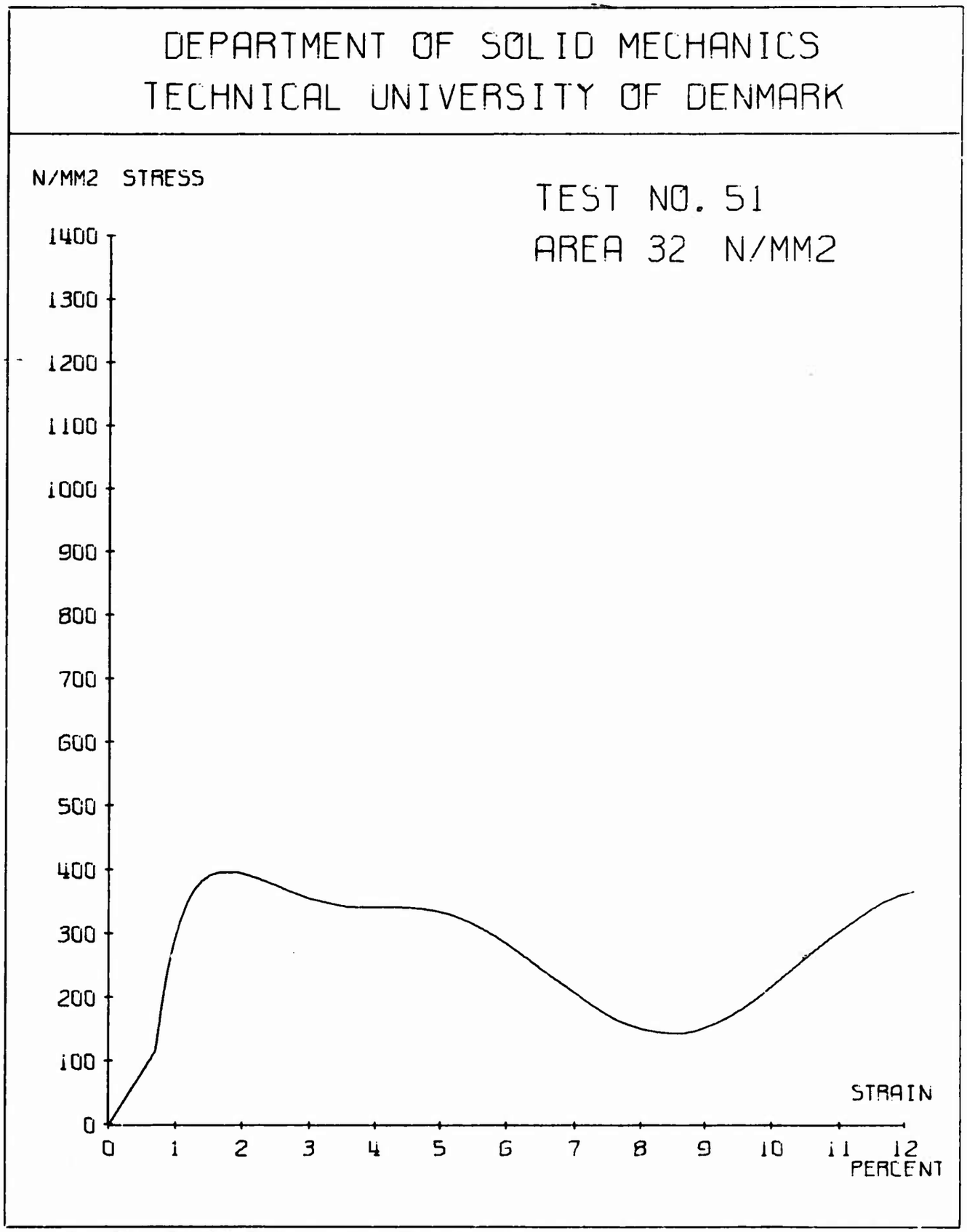

Fig. 23 - Stress-Strain Curve, Test No. 51

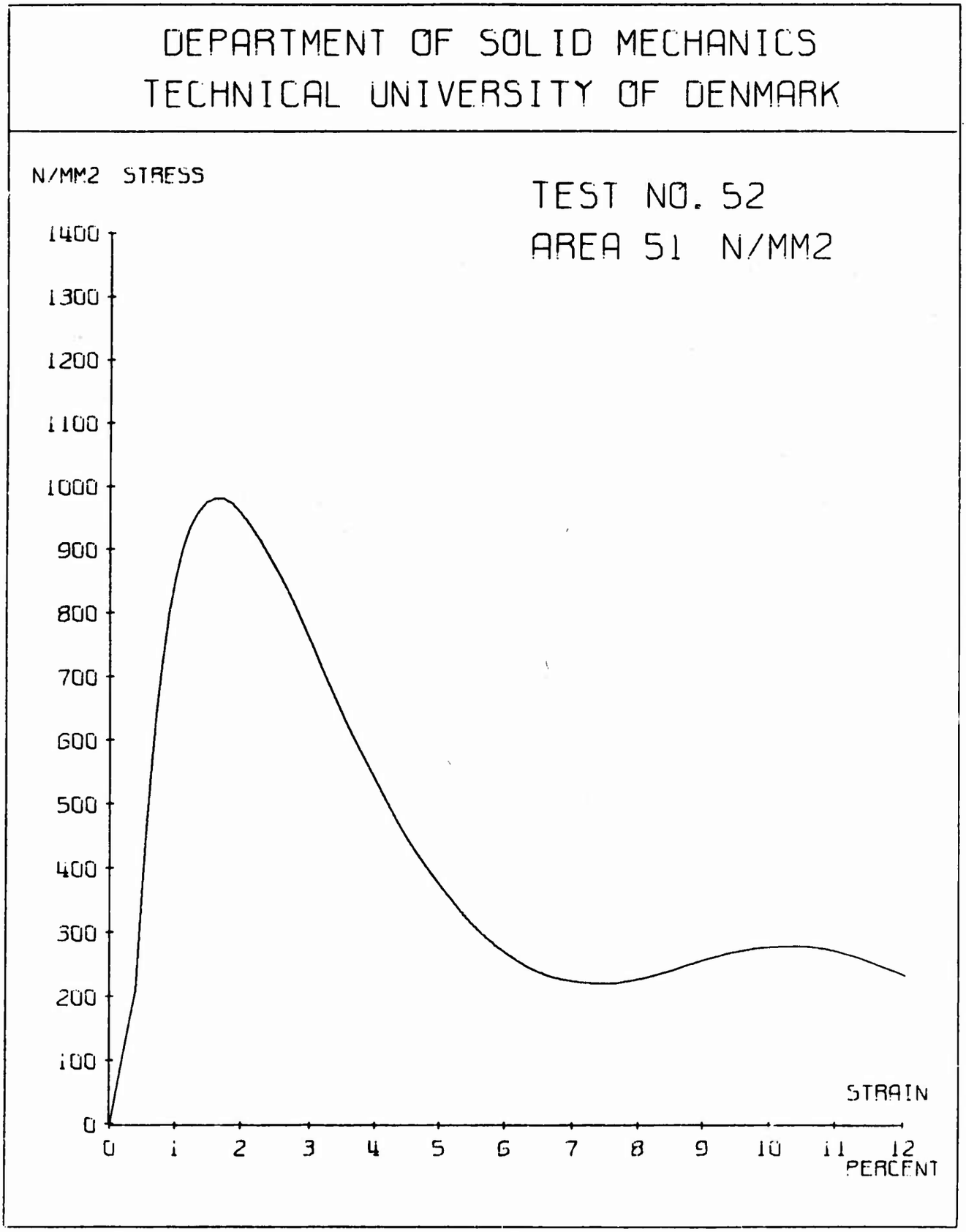

Fig. 24 - Stress-Strain Curve, Test No. 52

Series II

The results of the tests on annealed copper are reported in graphs 49-52. Except for the test No. 51, in which the counter gave erroneous results and which should therefore be discarded, the results show general agreement. The average value of the (maximum) strain rate was 2105 sec^{-1} and it varied no more than within about 3 per cent. The peak stress at roughly 2 per cent strain varies between 550 and 1000 N/mm^2 . The stress falls again to about 200 N/mm^2 at about 5-6 per cent strain, and it does not seem to rise appreciably again. None of the specimens fractured in this test but deformed to about 216 mm diameter corresponding to approx. 50 per cent linear elongation.

We computed the mechanical work done on the specimens up to 12 per cent elongation. From this figure a mean value of the stress may be found. For the tests in the first series (I) we found 44 N/mm^2, corresponding to a mean stress of 367 N/mm^2 . The corresponding figure for the annealed specimens (Series II) is 400 N/mm^2, but the variation is considerable.

IX. CONCLUSION

It is not easy to evaluate the method proposed for high strain rate tension tests. We have found the following advantages or points of credit:

1) High strain rates are easily obtained.
2) The strain rate does not vary considerably.

3) The strain field is unaxial and homogeneous.
4) It is easy to vary the strain rate within certain limits (not too low strain rates).

On the other hand, we should like to make it clear that the method presents certain difficulties. These can be summarized by saying that the determination of the resultant force is complicated by difficulties encountered in the measurement and analysis of the magnetic force and, to some extent, the inertia forces. We think that we have solved some of these difficulties and that the results that we were able to obtain are reliable but more work must be done here before the method becomes entirely satisfactory i.e. before the resulting stresses can be determined with a higher degree of accuracy.

REFERENCES

1. Kolsky, H., Proc.Phys.Soc., B 62, 676 (1949).
2. Alder, J.F., and Phillips, V.A., J.Inst.Metals, 83, 80 (1954).
3. Baron, H.G., J.Iron St.Inst., 182, 354 (1956).
4. Davies, E.D.H., and Hunter, S.C., J.Mech.Phys.Solids, II, 155 (1963).
5. Larsen, T.L., Rajnak, S.L., Hauser, F.E., and Dorn, J.E., J.Mech.Phys.Solids, 12, 361 (1964).
6. Hauser, F.E., Simmonds, J.A., and Dorn, J.E., Response of Metals to High Velocity Deformation, Interscience, N.Y., 93 (1961).
7. Hauser, F.E., Exp.Mech., 6, 395 (1966).
8. Dharan, C.K.H., and Hauser, F.E., Exp.Mech., 10, 370 (1970).
9. Niordson, F., Exp.Mech., 5, 29 (1965).

TABLE I

Outer radius R mm	Measured L_{12} µH	Calculated L_{12} µH	Rel. deviation D %
71.05	2.60	2.58	0.77
73.50	2.38	2.39	-0.42
76.10	2.18	2.20	-0.92
78.45	2.04	2.05	-0.49
80.85	1.91	1.91	0
83.20	1.80	1.80	0
85.90	1.70	1.68	1.18
88.10	1.61	1.61	0
90.85	1.54	1.53	0.65
93.30	1.47	1.48	-0.68

$$L_{12} = 16.1818 - 0.29955\ R + 0.0015221\ R^2$$

(L_{12} in µH , R in mm)

TABLE II

Outer radius R mm	Measured L_{23} nH	Calculated L_{23} nH	Rel. deviation D %
71.05			
73.50	12.5	12.5	0
76.10	20.6	20.4	0.97
78.45	27.5	27.5	0
80.85	34.3	34.7	-1.17
83.20	41.6	41.7	-0.24
85.90	49.8	49.6	0.40
88.10	56.3	56.0	0.53
90.85	63.7	63.9	-0.31
93.30	70.6	70.9	-0.42

$$L_{23} = \begin{cases} 1833.704 - 52.6097\ R + 0.378667\ R^2 & R \leq 73.5 \text{ mm} \\ -240.5133 + 3.8316\ R - 0.005288\ R^2 & R \geq 73.5 \text{ mm} \end{cases}$$

(L_{23} in nH , R in mm)

For the measurement the following instruments were used:

FLUKE Differential Voltmeter, 887 AB { DC: ±0.0025% of input; AC: ±0.05% of input

FLUKE Differential Ammeter, 853 A { DC: ±0.2% of input; AC: 0.5% of input